Electronic Supplementary Material (ESI) for ChemComm.

An Integrated Re(I) Photocatalyst/Sensitizer that Activates the Formation of Formic Acid from Reduction of CO_2

Yasmeen Hameed, Patrick Berro, Bulat Gabidullin and Darrin Richeson

Department of Chemistry and Biomolecular Sciences, Centre for Catalysis Research and Innovation
University of Ottawa, 10 Marie Curie, Ottawa, ON K1N 6N5

Table of Contents

Experimental Procedures

General Procedures. Reagents and analytical grade solvents were purchased from Strem Chemicals or Sigma Aldrich and used without further purification. The ^{1}H, $^{13}C\{^{1}H\}$ and $^{31}P\{^{1}H\}$ NMR spectra were recorded at 400, 100 and 162 MHz respectively with chemical shifts reported in ppm using the residual protons of the NMR solvent as internal standards.

Synthesis of *cis*-$Re(CO)_2(bipy)_2^+OTF^-$ Complex 1[7]

The complex *cis*-$[Re(CO)_2(bpy)_2](CF_3SO_3)$ was synthesized according to the literature from the *fac*-$Re(bpy)(CO)_3(CF_3SO_3)$ complex **A**. Complex **A** (1.895 g, 3.294 mmol)) was mixed with a large excess of bpy (≈2.0g) with a magnetic stir bar in a Schlenk tube, which was capped with a septum and purged with N_2. The reaction mixture was magnetically stirred and heated to reflux for 4 h during which time a red solid appeared. The reaction mixture was cooled and then dissolved in CH_2Cl_2 and transferred from the tube to a round bottom flask to remove the solvent under the vacuum. Purification was achieved by column chromatography on acidic alumina with CH_2Cl_2/CH_3CN mixtures. Yield: 1.526 g (83%). The ^{1}H NMR, UV-visible IR spectra and FAB-MS matched with the reported complex.31 ^{1}H NMR (δ/ppm, CD_3CN): 9.45 (d, 2H, J = 5.0 Hz), 8.48 (d, 2H, J = 8.6 Hz), 8.40 (d, 2H, J = 8.6 Hz), 8.15 (dt, 2H, J = 1.5, 8.1 Hz), 8.02 (dt, 2H, J = 1.5, 8.1 Hz), 7.63 (m, 2H), 7.41 (dd, 2H, J = 1.0, 5.5 Hz), 7.34 (m, 2H). UV-visible (λ (nm), CH_2Cl_2) (ϵ in M^{-1} cm^{-1}): 288 (47400), 364 (6100), 400 (6590), 492 (5320), 564 (sh, 3660). IR (CH_2Cl_2) (ν(CO), cm^{-1}): 1992, 1852. FAB-MS^+: 555.08. ^{13}C -NMR (CD_3CN): δ 117.3, 123.9, 124.8, 127.3, 128.1, 137.6, 139.5, 147.8, 155.8, 200.3. Analysis cald for $C_{23}H_{16}F_3N_4O_5ReS$: C, 39.26; H, 2.29; N, 7.96; Found: C 39.34; H 2.13; N 8.06.

Crystals suitable for X-ray analysis were grown by diffusion of saturated CH_2Cl_2 solution in CH_3CN. The structure of the rhenium (I) dicarbonyl compound is shown in Figure **S1**.

Typical Photocatalytic Experiments: A 20 mL glass vial with a magnetic stir bar was charged, in a nitrogen filled glovebox, with 4mL of a solvent dimethylacetamide (DMA) or acetonitrile (MeCN) or N,N-dimethylformamide (DMF) that contained catalyst, photosensitizer ($[Ru(bpy)_3](PF_6)_2$), and approx. 1mL triethanolamine (TEOA) as an electron donor. The vial was sealed and removed from the glovebox. The solution was purged with CO_2 for 15 minutes and irradiated using a 405 nm LED light (radiant flux at 700 mA of 1050 mW) for 24 hours. The light intensity was measured to be $3.4x10^{-8}$ moles photons/s using a $Ru(bpy)_3^{2+}$/1,9-diphenylanthracene (DPA) actinometer.[1,2] After irradiation, carbon monoxide and hydrogen production were measured using an Agilent 7820A gas chromatograph (GC) with an Agilent select permanent gases column and equipped with a thermal conductivity detector (TCD). The liquid products from the photocatalytic reactions were analyzed using ^1H NMR. A calibration curve for formic acid was prepared in D_2O containing dimethyl sulfone as an internal standard. An aliquot (100μL) was removed from the irradiated samples and was mixed in an NMR tube with D_2O containing a known amount of dimethyl sulfone (400 μL). The sample was mixed well and the ^1H NMR spectra were collected. Using the integrated values for the formic acid ($\delta \approx$ 8.1ppm) and a calibration curve, the amount of formic acid was determined. High resolution mass spectrometry for analysis of ^{13}CO and $H^{13}COOH$ was performed using a Kratos Concept 1S HiRes Electron Impact Magnetic Sector Mass Spectrometer using a inlet system in the John L. Holmes Mass Spectrometry Center at the University of Ottawa. A similar experiment was carried out using catalyst employing $^{13}CO_2$ (99% ^{13}C and <3% ^{18}O from Sigma-Aldrich) at a pressure was 20 PSI. The mixture was stirred and exposed to 405 nm blue LED for 24 h, and the gas phase products were analyzed as described.

Electrochemistry: Electrochemical experiments were carried out in a single compartment cell wrapped with aluminum foil using a VersaSTAT 3 (Princeton Applied Research) potentiostat. Samples were prepared in a glovebox, sealed, removed from the glovebox and connected to a

Schlenk line and maintained under a nitrogen atmosphere. A conventional three electrode system was employed consisting of a glassy carbon working electrode (diameter = 0.3 cm), a Pt wire as the auxiliary electrode, and an Ag wire as a pseudo-reference electrode. Ferrocene was added as a reference compound and potentials were referred to the redox potential of ferrocene (Fc)/ferrocenium ion (Fc^+) as an internal standard. Dried acetonitrile was purchased from Sigma Aldrich and stored on molecular sieves in glove-box. Tetrabutylammoniumhexafluorophosphate, $[(n\text{-}Bu)_4N]PF_6$ (TBAHFP), the supporting electrolyte, was crystallized two times with methanol, dried in vacuum at 90 °C for 24 h before used and stored in a glovebox. The electrolyte solution, 0.1 M $[(n\text{-}Bu)_4N]PF_6$ in CH_3CN, was saturated with N_2 by purging with N_2 for 10 min prior to each experiment. The typical concentration of catalyst was 1 mM (15 mL acetonitrile) in each experiment.

X-ray Crystallography: The crystals were mounted on thin glass fibers using paraffin oil. Prior to data collection crystals were cooled to 200.15 °K. Data were collected on a Bruker AXS SMART single crystal diffractometer equipped with a sealed Mo tube source (wavelength 0.71073 Å) APEX II CCD detector. Raw data collection and processing were performed with APEX II software package from BRUKER AXS.[3] Initial unit cell parameters were determined from 60 data frames with 0.3° ω scan each collected at the different sections of the Ewald sphere. Semi-empirical absorption corrections based on equivalent reflections were applied.[4] Systematic absences in the diffraction data-set and unit-cell parameters were consistent with the assigned space group. The structures were solved by direct methods, completed with difference Fourier synthesis, and refined with full-matrix least-squares procedures based on F^2. All hydrogen atoms positions were calculated based on the geometry of the related non-hydrogen atoms. All hydrogen atoms were treated as idealized contributions during the refinement. All scattering factors are contained in several versions of the SHELXTL program library, with the latest version used being v.6.12.[5]

Computational Details: Optimized structures were obtained from density functional theory (DFT) computations using Gaussian 09.[6] The B3LYP functional and def2TZVP basis set was used for all atoms.

Emission-Quenching Experiments

The emission-spectra was obtained according to similar procedure in the reported literature.[2] In a nitrogen filled glovebox, solutions of the photosensitizer $Ru(bpy)_3(PF_6)_2$ (0.1 mM) in anhydrous acetonitrile were prepared containing different concentrations of the quencher. The steady-state emission spectrum (excitation wavelength 450 nm) of each solution was recorded, and the intensity of the luminescence for the ^{3}MLCT excited state of the photosensitizer (452 nm) was recorded.

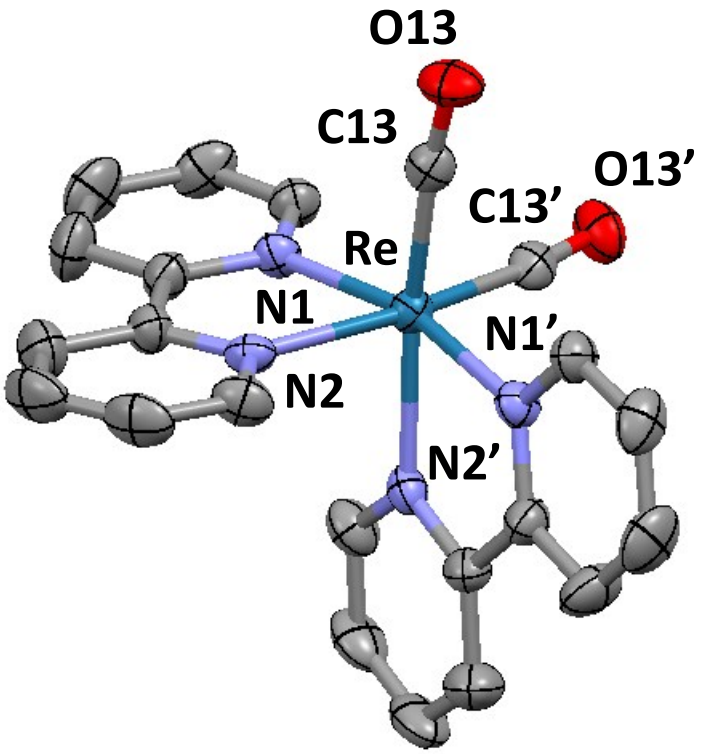

Figure S1. Structural representation for the cation of compound ***cis*-Re(CO)$_2$(bipy)$_2^+$OTf$^-$ (1$^+$OTf$^-$)** obtained from X-ray analysis. Hydrogen atoms are omitted for clarity.

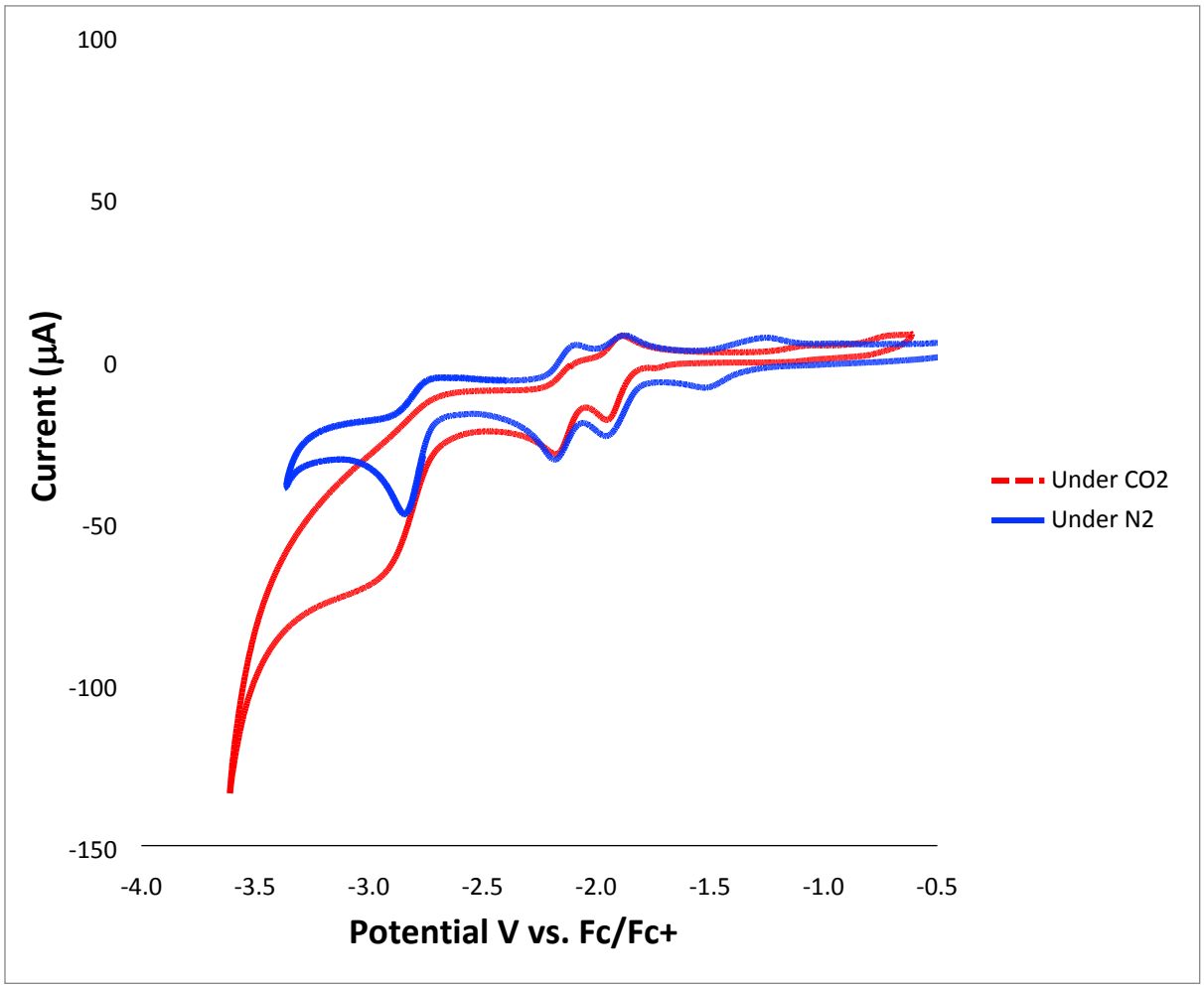

Figure S2. The cyclic voltammagram under reducing potentials of *cis*-$Re(CO)_2(bipy)_2^+OTf^-$ (1.0 mM) under N_2 (blue) OR CO_2 (red) in CH_3CN with 0.1M tetrabutylammoniumhexafluorophosphate (TBAHFP) supporting electrolyte at a scan rate of 100 mV/s. Reference to Fc/Fc^+.

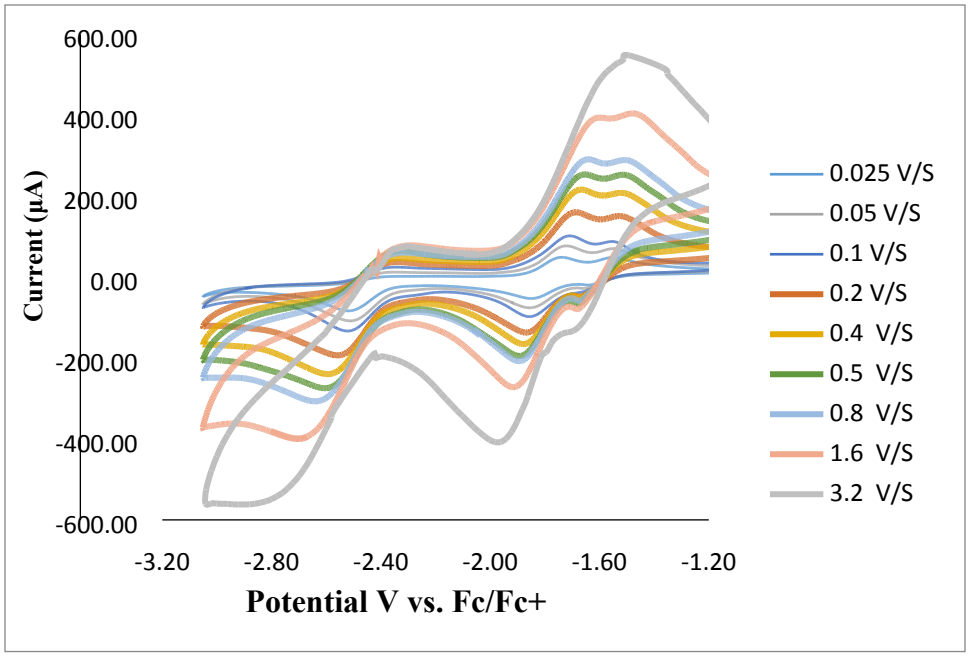

Figure S3. Cyclic voltammograms for *cis*-$Re(CO)_2(bipy)_2^+OTf^-$ (1.0 mM) under N_2 in CH_3CN with 0.1M tetrabutylammonium hexafluorophosphate (TBAHFP) supporting electrolyte with different scan rates.

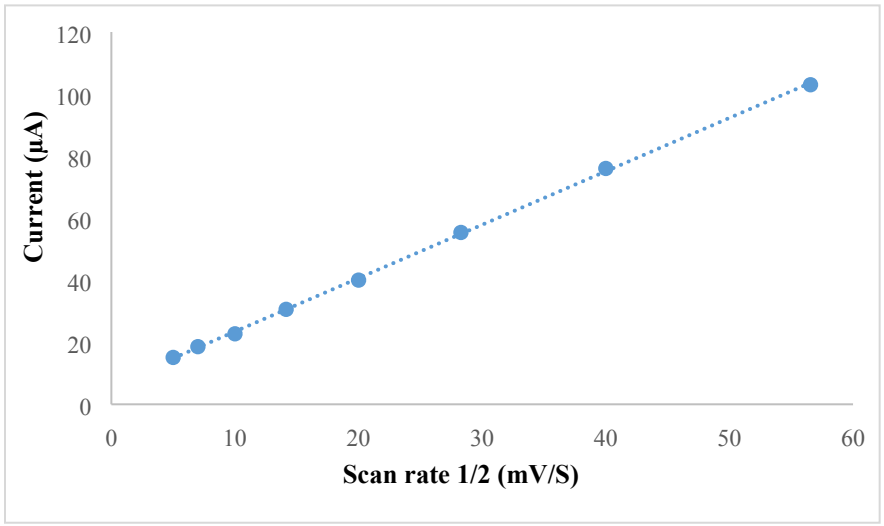

Figure S4. Plot of scan rate$^{1/2}$ versus current for the first reduction peak.

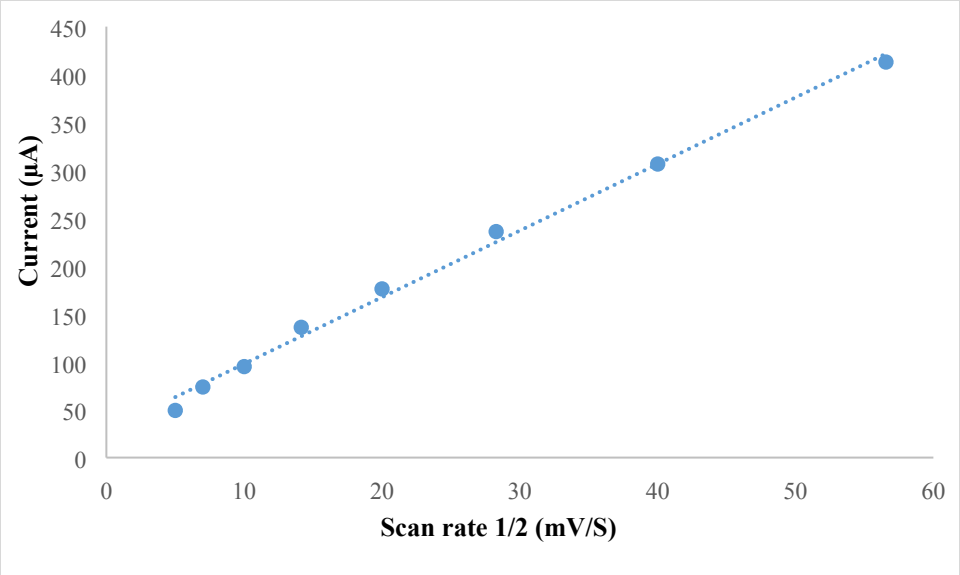

Figure S5. Plot of scan rate$^{1/2}$ versus current for second reduction peak.

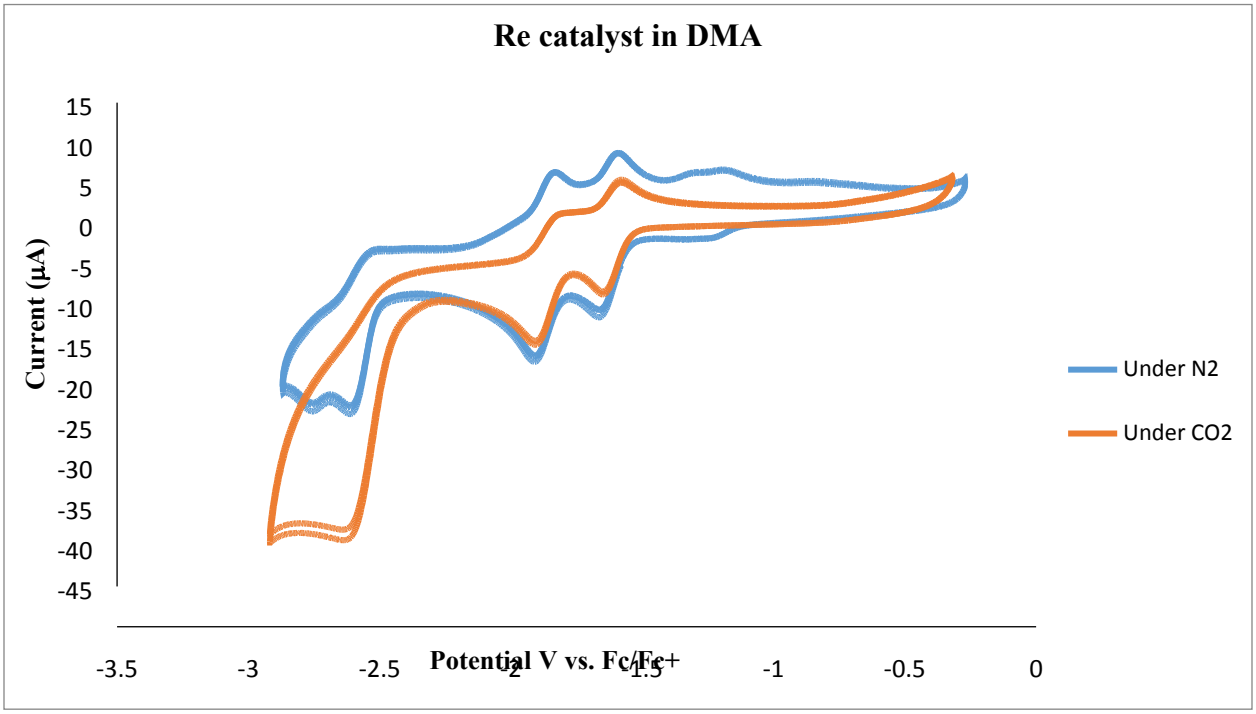

Figure S6. The cyclic voltammagram under reducing potentials of *cis*-$Re(CO)_2(bipy)_2^+OTf^-$ (1.0 mM) under N_2 (blue) OR CO_2 (red) in DMA with 0.1M tetrabutylammoniumhexafluorophosphate (TBAHFP) supporting electrolyte at a scan rate of 100 mV/s. Reference to Fc/Fc^+.

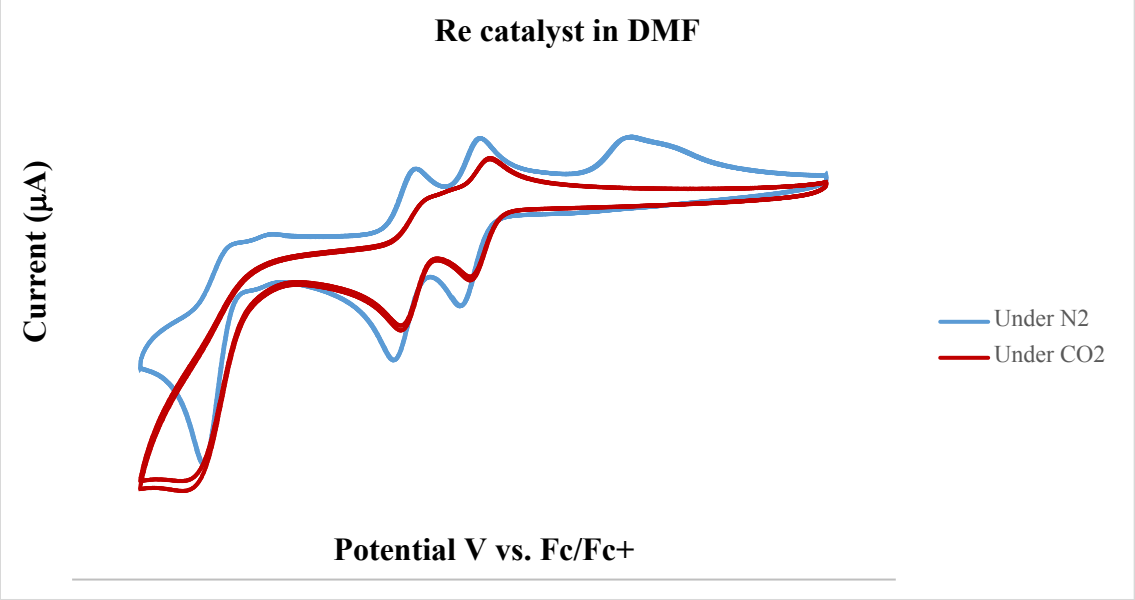

Figure S7. The cyclic voltammagram under reducing potentials of *cis*-$Re(CO)_2(bipy)_2^+OTf^-$ (1.0 mM) under N_2 (blue) OR CO_2 (red) in DMF with 0.1M tetrabutylammoniumhexafluorophosphate (TBAHFP) supporting electrolyte at a scan rate of 100 mV/s. Reference to Fc/Fc^+.

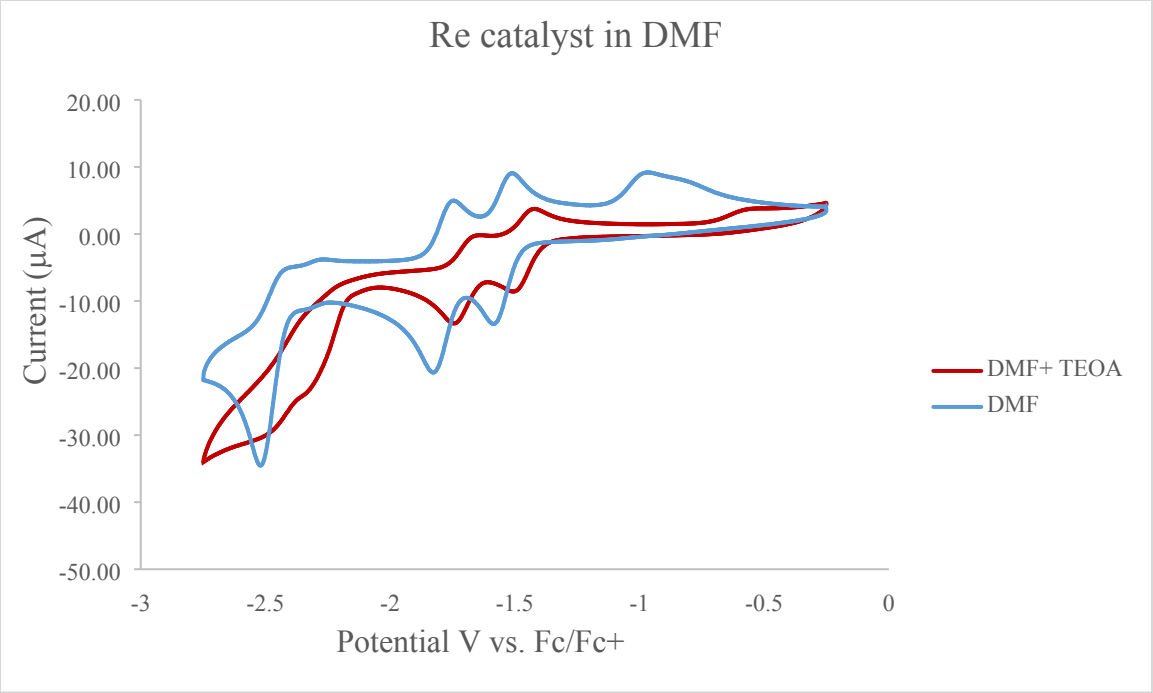

Figure S8. The cyclic voltammagram under reducing potentials of *cis*-$Re(CO)_2(bipy)_2^+OTf^-$ (1.0 mM) under N_2 DMF (blue) or in DMF/TEOA (red) with 0.1M tetrabutylammoniumhexafluorophosphate (TBAHFP) supporting electrolyte at a scan rate of 100 mV/s. Referenced to Fc/Fc^+.

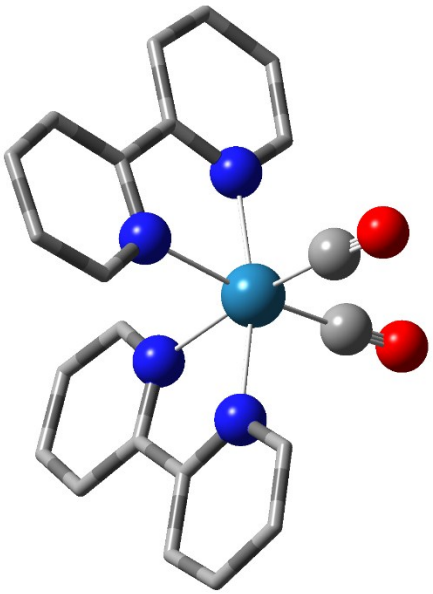

Figure S9. A ball and stick structural representation for the computationally optimized $[Re(CO)_2(\kappa^2\text{-bpy})_2]^+$ compound **1**$^+$. DFT calculations used the B3LYP functional and the def2TZVP basis set. Hydrogen atoms are not shown for clarity. Some carbon atoms have been removed for clarity.

Table S1. A comparison of metal–ligand distances (Å) from the experimental single crystal X-ray analysis and from the computationally optimized structures (**1**) and and the single electron reduction product (**A**).

Bond /cmpd	$[Re(\kappa^2\text{-}bpy)_2(CO)_2]^+$ (**1**$^+$) X-ray analysis	$[Re(\kappa^2\text{-}bpy)_2(CO)_2]^+$ (**1**$^+$) Computed	Reduced complex $[Re(\kappa^2\text{-}bpy)_2(CO)_2]$ (**A**) Computed
M-N trans CO	2.165(3)	2.215	2.2028
M-N trans N	2.121(3)	2.147	2.1319
M-CO	1.883(5)	1.921	1.9156
N-M-N_{py}	75.15(13	74.67	75.326

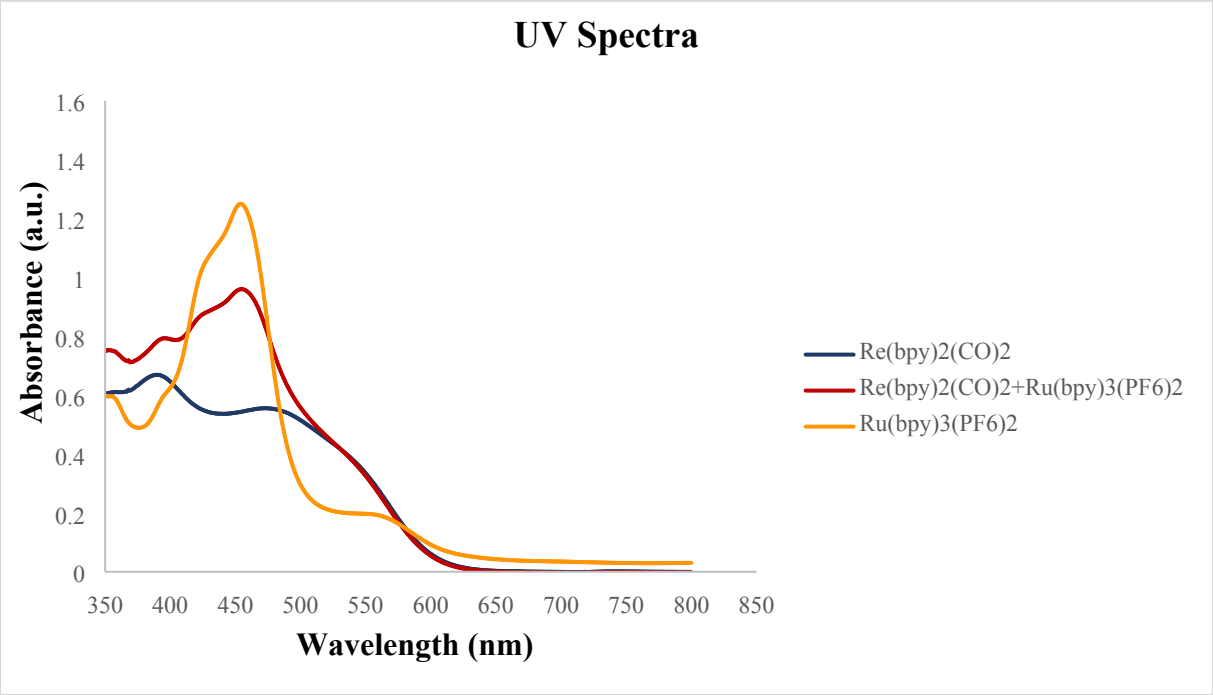

Figure S10. Uv-vis of complexes $[Re(CO)_2(\kappa^2\text{-bpy})_2]^+OTf^-$ (black), $[Ru(bpy)_3](PF_6)_2$ (yellow) and a combination of these two complexes (red). Spectra obtained in CH_2Cl_2 solvent.

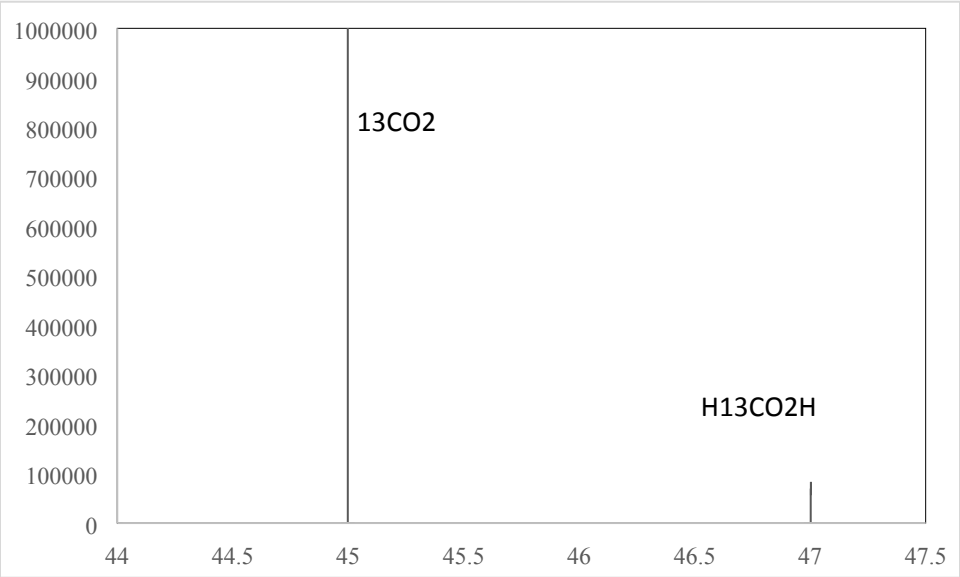

Figure S11. High resolution MS of the headspace of a photocatalytic reduction experiment in DMF using $^{13}CO_2$ with complex $[Re(CO)_2(\kappa^2\text{-bpy})_2]^+OTf^-$ as catalyst. Mass peaks for $H^{13}CO_2H$, $^{13}CO_2$ are indicated.

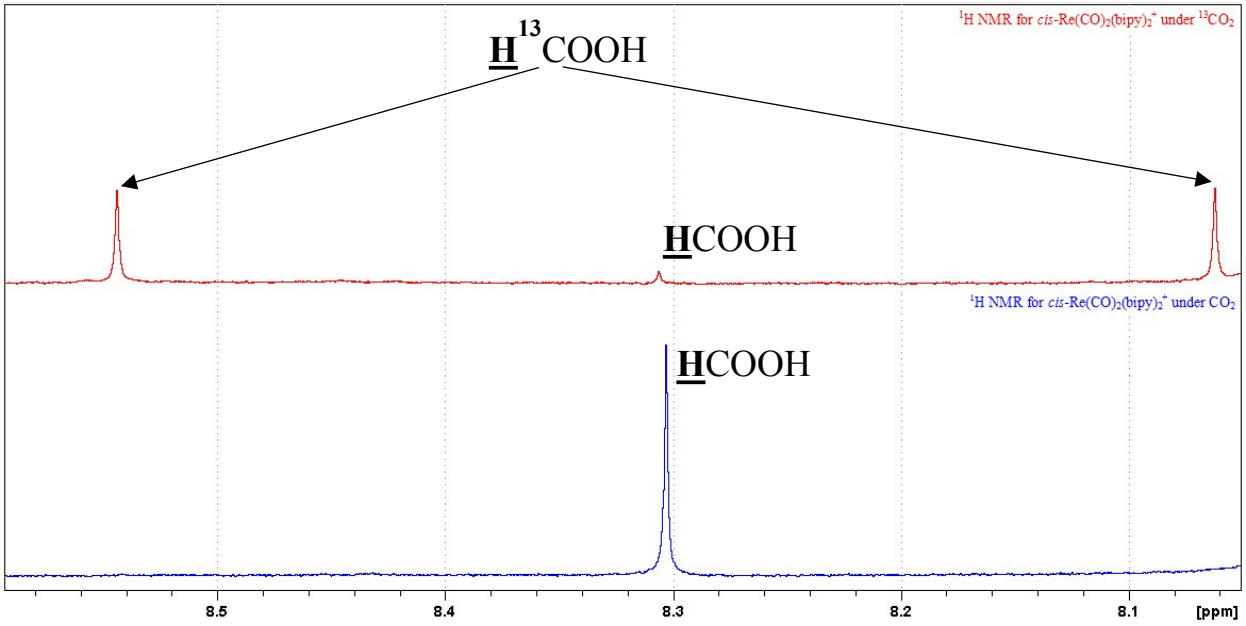

Figure S12. ^{1}H NMR spectra for the formyl HOOC-**H** proton of formic acid obtained from photocatalytic reduction of CO_2 using *cis*-[Re(CO)$_2$(κ^2-bpy)$_2$]$^+$OTf $^-$ as the catalyst. The bottom spectrum was from reaction using unlabeled CO_2 and the top spectrum is from a reaction with labeled $^{13}CO_2$.

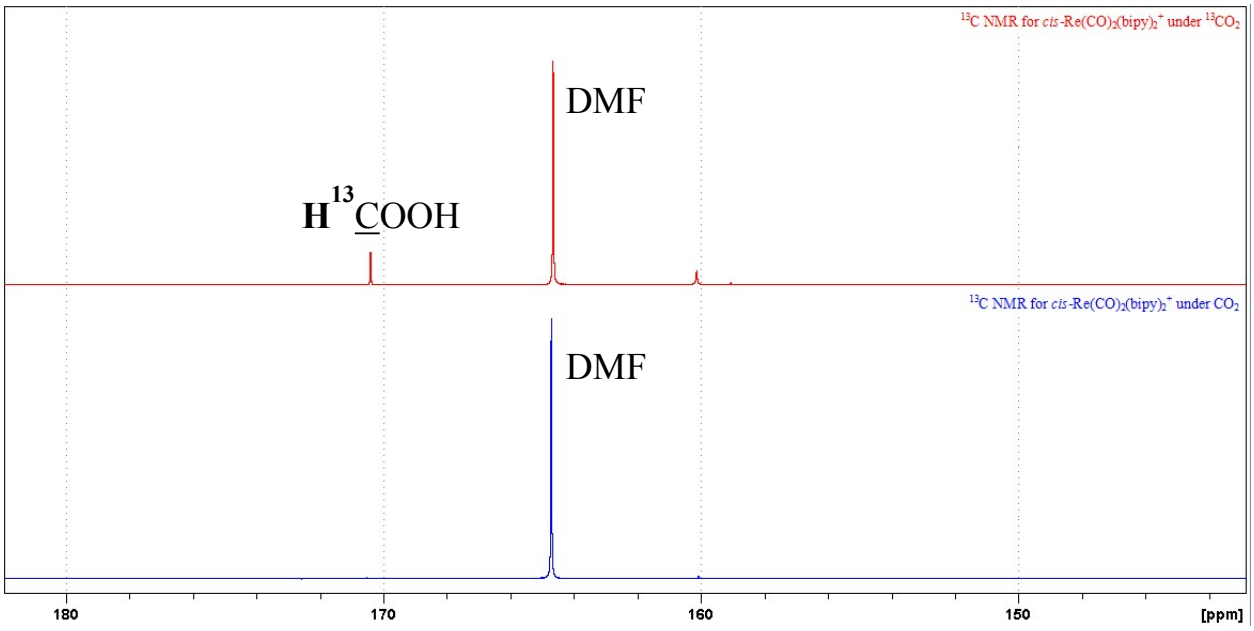

Figure S13. ^{13}C NMR spectra in D_2O for the photocatalytic reduction of $^{13}CO_2$ (top) to produce formic acid using *cis*-Re(CO)$_2$(bipy)$_2^+$OTf $^-$ as the catalyst. For comparison, a reaction using unlabeled CO_2 (bottom) is shown.

Table S2. Summary of results for the photocatalytic CO_2 reduction with $[Re(CO)_2(\kappa^2\text{-bpy})_2]^+OTf^-$ (**1^+OTf^-**) in dimethylformamide (DMF), dimethylacetamide (DMA) and acetonitrile (CH_3CN).Irradiation with 405 nm light conducted on solution under a CO_2 atmosphere for 24 h. Electron donor used was triethanolamine (TEOA).

Catalyst (μmol)	$Ru(bpy)_3^{2+}$ (μmol)	Solvent	H_2 (μmol)	TON (H_2)	HCOOH (μmol)	TON (HCOOH)	Selectivity
-	4	DMA	7	1.75[a]	50	12.5[a]	87%
-	4	DMF	8	2[a]	60	15[a]	88%
-	4	CH_3CN	6	1.5[a]	10	2.5[a]	63%
4	-	DMA	-	-	41	10.3	100%
4	4	DMA	6	1.5	208[a]	52	97%
4	-	DMF	3	0.8	43	10.8	93%
4	4	DMF	11	2.8	262[a]	66	96%
4	-	CH_3CN	-		-	-	-
4	4	CH_3CN	11	2.8	46[a]	11.5	80%

[a] TON based on $Ru(bpy)_3^{2+}$

[b] corrected for background due to $Ru(bpy)_3^{2+}$

Table S3. The time profile for the CO_2 photocatalytic reduction using $[Re(CO)_2(\kappa^2\text{-bpy})_2]^+OTf^-$ (**1^+OTF^-**) with $Ru(bpy)_3^{2+}$ as **PS** in dimethylformamide (DMF). Irradiation with 405 nm light conducted on solution under a CO_2 atmosphere. Electron donor used was triethanolamine (TEOA).

Time (h)	H_2	TON $_{H2}$	HCOOH	TON $_{HCOOH}$	Selectivity for HCOOH
0	0	0	0	0	-
8	4	1	50	12.5	0.93
12	10	2.5	78	19.5	0.89
24	11	4.5	202	50.5	0.95
48	24	6	238	59.5	0.91
72	34	8.5	277	69.25	0.89

Table S4. Summary of results for the photocatalytic CO_2 reduction with $[Re(CO)_2(\kappa^2\text{-bpy})_2]^+OTf^-$ (**1^+OTf^-**) in dimethylformamide (DMF) or dimethylacetamide (DMA) using added proton sources of either H_2O or phenol. Irradiation with 405 nm light conducted on solution under a CO_2 atmosphere for 24 h. Electron donor (approx. 1mL) used was triethanolamine (TEOA) or trimethylamine (TEA).

Catalyst (□mol)	**$Ru(bpy)_3^{2+}$ (□mol)**	**Solvent**	**ED**	**Additive**	**H_2 (μmol)**		**HCOOH (μmol)**
4	4	DMF	TEOA	H_2O (0.5mL)	17		100
4	4	DMF	TEOA	H_2O (1mL)	23		103
4	4	DMF	TEOA	Phenol (0.5g)	21		108
	4	DMF	TEOA	Phenol (1g)	23		76
4	4	DMF	TEA	H_2O (0.5mL)	8		50
4	4	DMF	TEA	H_2O (1mL)	11		58
4	4	DMF	TEA	Phenol (0.5g)	4		41
4	4	DMF	TEA	Phenol (1g)	65		45
4	4	DMA	TEOA	H_2O (0.5mL)	13		82
	4	DMA	TEOA	H_2O (1mL)	14		96
4	4	DMA	TEOA	Phenol (0.5g)	31		120
4	4	DMA	TEOA	Phenol (1g)	36		139

Table S5. Effects of different concentration of catalyst *cis*-$[Re(CO)_2(bipy)_2]^+OTf^-$ (**1^+OTF^-**) for the photocatalytic reduction of CO_2. Reaction conditions: DMA: TEOA (4:1) 4 mL; photosensitizer $[Ru(bpy)_3]^{2+}$ (1mM) under CO_2 atmosphere.

Catalyst (mM)	H_2 (µmol)	TON (H_2)	HCOOH (µmol)	TON (HCOOH)	selectivity	HCOOH rate /hr	TOF hr-1
1[a]	-	-	41	10.3	1	1.7	0.43
1	6	1.5	208	52	0.97	8.7	2.2
0.5	29	15	229	115	0.89	9.5	4.8
0.2	19	24	220	275	0.92	9.2	11.5
0.1	15	38	171	428	0.92	7.1	17.8
0.05	10	50	107	535	0.91	4.5	22.3
0.02	18	225	118	1480	0.87	4.9	61.5
0.01	15	375	110	2750	0.88	4.6	114.6

[a] No added $Ru(bpy)_3^{2+}$

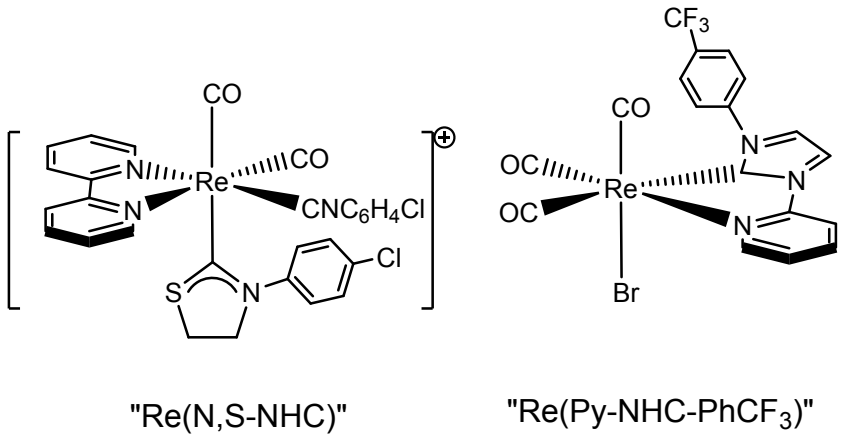

Figure S14. Representations of Re(*N*,*S*-NHC) and Re(Py-NHC-PhCF$_3$) presented in Table 1 of the manuscript.

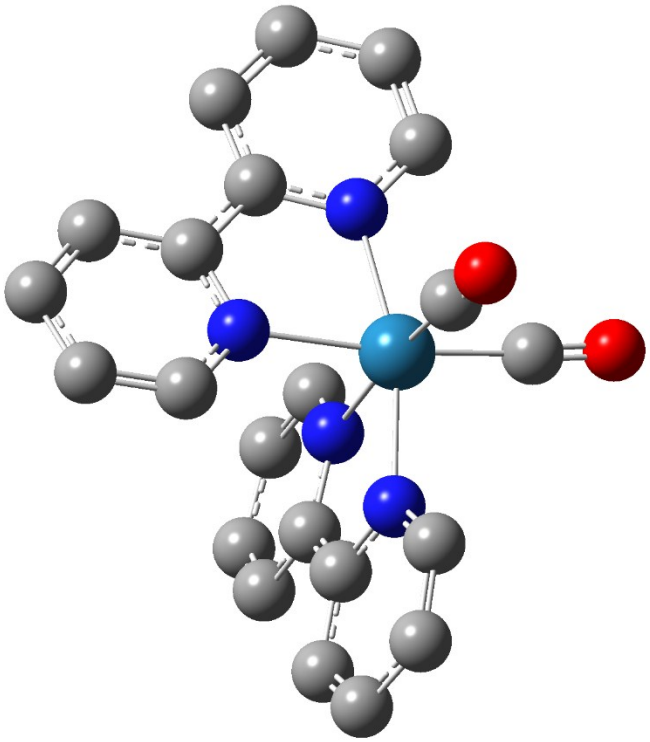

Figure S15. A ball and stick structural representation for the computationally optimized [Re(CO)$_2$(κ^2-bpy)$_2$] compound **A**. DFT calculations used the B3LYP functional and the def2TZVP basis set. Hydrogen atoms are not shown for clarity. Some carbon atoms have been removed for clarity.

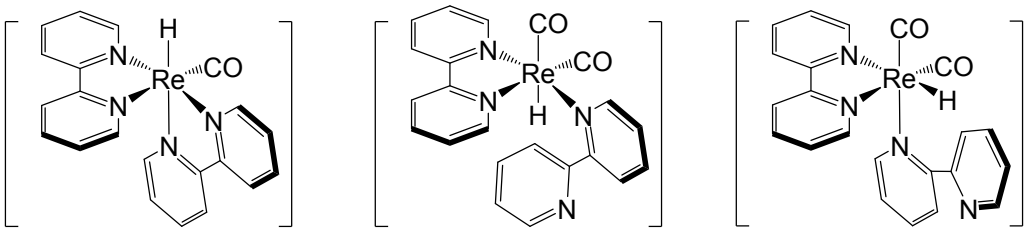

-1296.80983 -1296.730545 -1296.738012

Figure S16. Representations of the three possible protonation products to yield Re-H intermediates that may arise in the catalytic cycle shown in Figure 3 of the manuscript. Each of these species was computationally optimized as a means of determining the most likely structure of proposed **ReH**. DFT calculations used the B3LYP functional and the def2TZVP basis set (see Figures S14, S15). The results for the energies associated with each of these possibilities is indicated in Hartrees. This indicated that [Re(CO)(κ^2-bpy)$_2$H] was the lowest energy species and was thus used in the proposed cycle.

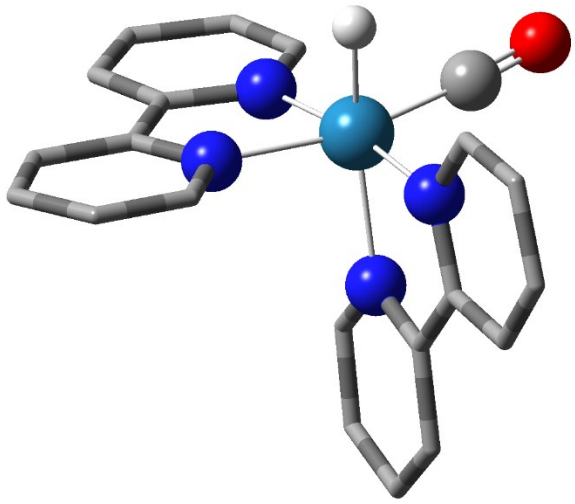

Figure S17. A ball and stick structural representation for the computationally optimized [Re(CO)(κ^2-bpy)$_2$H] compound **ReH**. DFT calculations used the B3LYP functional and the def2TZVP basis set. Hydrogen atoms are not shown for clarity. Some carbon atoms have been removed for clarity.

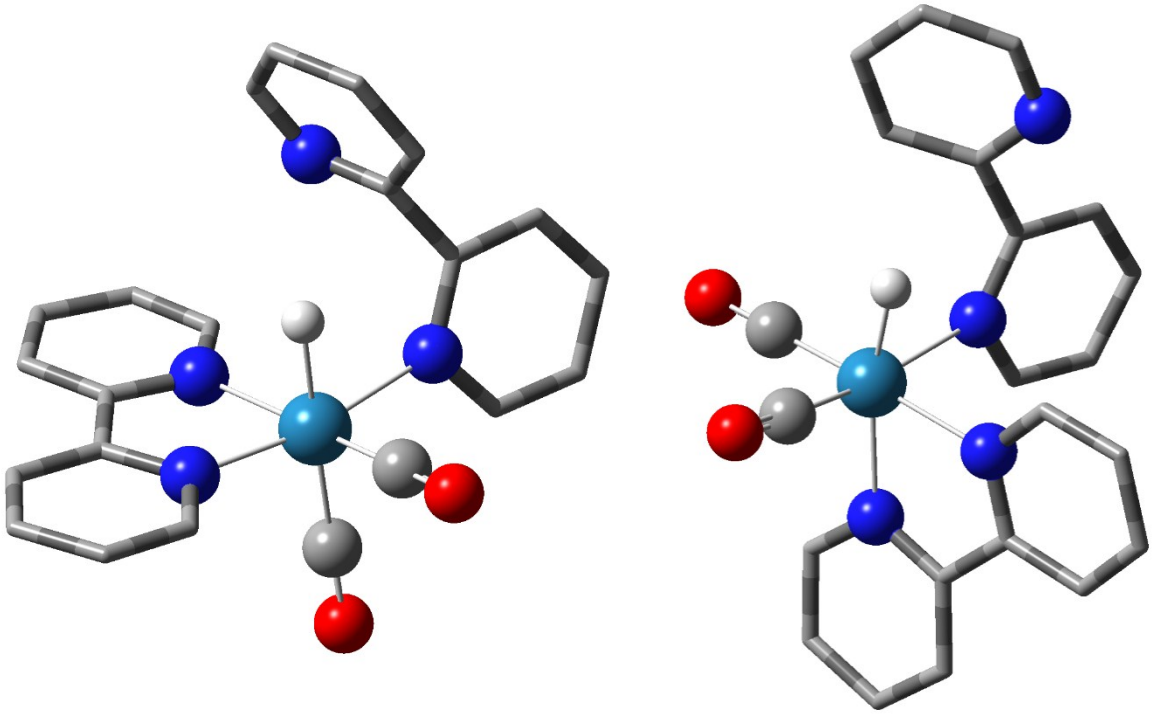

Figure S18. Ball and stick structural representations for the two isomers of the computationally optimized [$Re(CO)_2(\kappa^1$-bpy)(κ^2-bpy)H] compound as a proposed intermediate in the catalytic cycle (see Figure S13 and Figure 3). DFT calculations used the B3LYP functional and the def2TZVP basis set. Hydrogen atoms are not shown for clarity. Some carbon atoms have been removed for clarity.

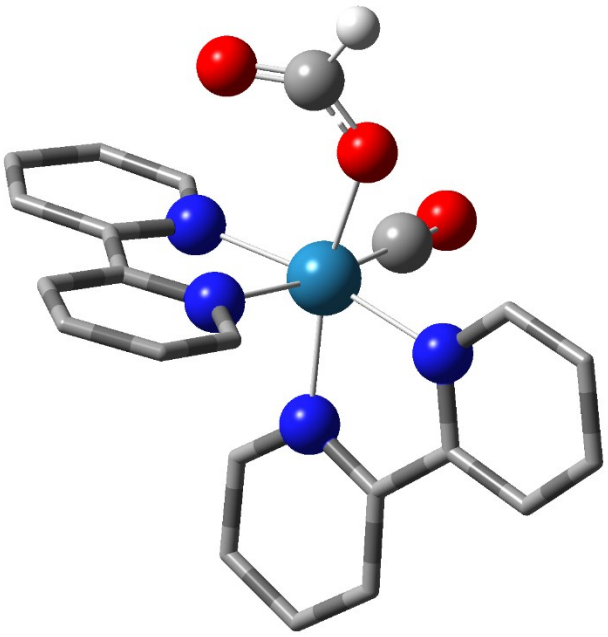

Figure S19. A ball and stick structural representation for the computationally optimized [Re(κ^2-bpy)$_2$(CO)(OC(O)H] compound **Re(form)**. DFT calculations used the B3LYP functional and the def2TZVP basis set. Hydrogen atoms are not shown for clarity. Some carbon atoms have been removed for clarity.

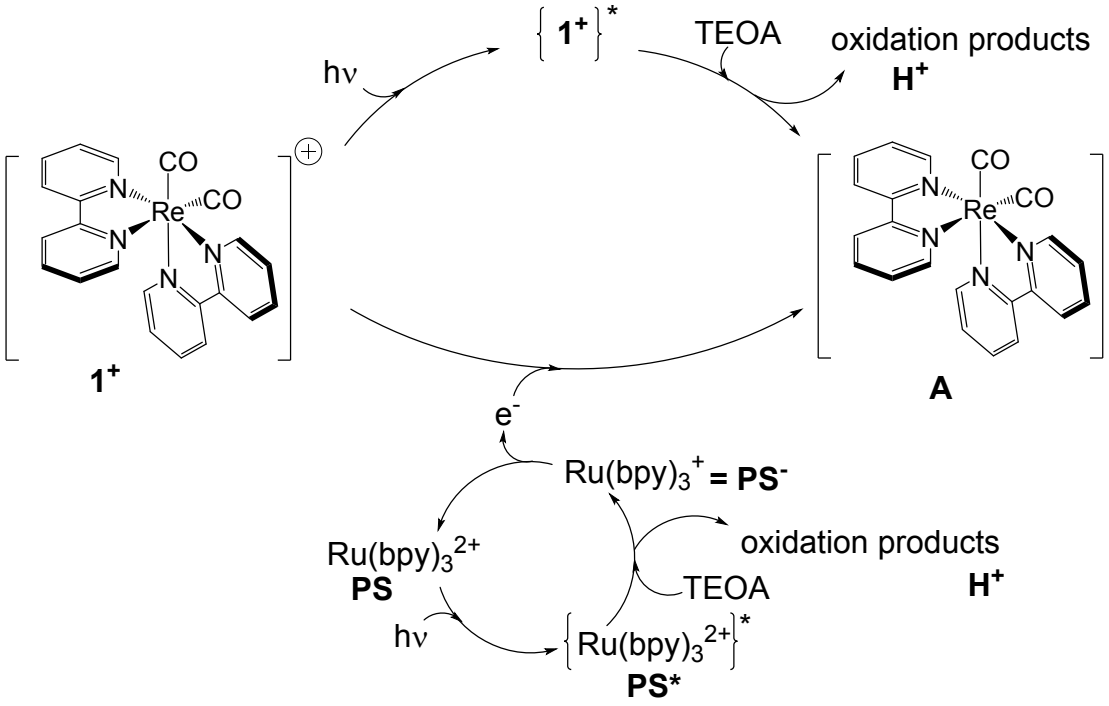

Figure S20. Additional details for the proposed reduction of **1**$^{+}$ to **A** providing entry into the catalytic cycle represented in Figure 3 of the manuscript text. The upper electron transfer process operates with **1**$^{+}$ as an integrated photosensitizer and catalyst. The electrons for the catalytic cycle come from reductive quenching by TEOA of the photoexcited **{1**$^{+}$**}***. The lower process represents the electron cycle that originates from the $Ru(bpy)_3^{2+}$ photosensitizer.

References:

[1] S. P. Pitre, C. D. McTiernan, W. Vine, R. Dipucchio, M. Grenier, J. C. Scaiano, *Sci. Rep.* **2015**, *5*, 1–10.

[2] Y. Hameed, B. Gabidullin, D. Richeson, *Inorg. Chem.* **2018**, *57*, 13092–13096.

[3] APEX Softward Suite v 2010 Bruker AXS Inc. Madison Wisconsin USA, **2010**.

[4] R. H. Blessing, *Acta Crystallogr. Sect. A* **1995**, 33–38.

[5] G. M. Sheldrick, *Acta Crystallogr. Sect. A* **2008**, 112–122.

[6] M. J. Frisch, G. W. Trucks, H. B. Schlegel, G. E. Scuseria, M. A. Robb, J. R. Cheeseman, G. Scalmani, V. Barone, G. A. Petersson, H. Nakatsuji, et al., **2016**.

[7] J. L. Smithback, J. B. Helms, E. Schutte, S. M. Woessner, B. P. Sullivan, *Inorg. Chem.* **2006**, *45*, 2163–74.

[8] T. N. Twala, A. Roodt, H. G. Visser, *Dalton Trans.* **2015**, *44*, 3278–3288.